Induced-moment singlet-triplet model: High-temperature series expansion

K. Rauchwarger, S. Jafarey, and Yung-Li Wang
Department of Physics, Florida State University,
Tallahassee, Florida 32306
(Received 31 July 1978)

We have obtained five terms in the high-temperature series expansion for the magnetic susceptibility for the singlet-triplet model, which has been used to represent, in a simplified version, the cubic induced-moment systems such as fcc Pr, Pr_3Tl, and TbSb. Our high-temperature series is valid for an arbitrary energy splitting between the singlet level and the triplet level. It also allows for arbitrary range of interaction and lattice geometry. The critical temperature as a function of the crystal field to the exchange-interaction ratio is estimated for the three cubic lattices of the nearest-neighbor interaction model. We show that the molecular-field predictions are unacceptable for induced-moment systems with the crystal-field to the exchange-interaction ratio near the critical value for magnetic ordering (at $T=0$) such as fcc Pr and Pr_3Tl.

I. INTRODUCTION

Crystal-field effects in magnetic systems have long been recognized. Indeed, the existence of the electrostatic crystalline potential can alter the magnetic behavior of the system in a fundamental manner. The most striking examples are the induced-moment systems where the crystal-field ground state is a singlet[1] or a nonmagnetic doublet.[2] In these compounds the transition temperature depends crucially on the ratio of the crystal-field strength to the exchange-interaction coupling. It has been shown both theoretically and experimentally that magnetic ordering would not exist, even at zero temperature, for the crystal-field to exchange-interaction ratio exceeding a critical value.[1] For higher values of exchange-interaction, magnetic moments are induced through a bootstrap process by mixing the excited crystal-field states into the ground state, similar to the occurrance of the Van Vleck paramagnetism. However, for the induced-moment magnetism the self-consistent exchange field takes the place of an externally applied magnetic field.

There has been a tremendous interest in the research of induced-moment systems in recent years. Most notably, inelastic-neutron-scattering measurements have been performed extensively in the study of these systems and have provided a great deal of information never attainable before; the neutron scattering measurement not only finds the crystal-field potential and the details of the exchange interactions, but also detects directly the fluctuations of the system. Today, in conjunction with measurements by other techniques, the neutron data can generally provide a very accurate experimental description of a magnetic system. The high accuracy of the experimental measurements in turn demands a more refined theoretical treatment. This is the situation we are experiencing in the study of rare-earth systems in general, and in particular the induced-moment systems.

Perhaps the simplest induced-moment system is the singlet-singlet model. There, each ion has a singlet crystal-field ground state and a singlet excited state separated by an energy gap. The exchange interaction prevailing between each pair of ions gives rise to a magnetic ordering at low temperatures for values of the interaction exceeding a critical value. The model provides a good approximation to $TbAsO_4$ and $TbVO_4$ for example; in these compounds a cooperative Jahn-Teller structural phase transition at a low temperature lowers the symmetry of the crystals from tetragonal to orthorhombic and leaves a pair of closely spaced low-lying singlet energy levels, for each Tb ion, almost completely isolated from the other energy levels.[3,4] Because of the relative simplicity of the model, extensive theoretical study has been invited.[5–7] Most recently the high-temperature series expansion has been carried out by several research groups.[7] The dependence of critical temperature on the crystal-field to exchange-interaction ratio has been accurately determined, and shows a gross inaccuracy of the molecular-field approximation.[7]

While the singlet-singlet model is most susceptible to theoretical studies, very few physical systems of such kind have been found and studied experimentally. On the other hand most of the experimental work on the induced-moment systems has been on dhcp Pr, fcc Pr, Pr_3Tl, $Pr_{3-x}La_xTl$, and TbSb.[8–12] These compounds, except the first one, all have a ground singlet and a first excited triplet as the two lowest-

lying crystal-field multiplets. A singlet-triplet model is thus more appropriate for describing these systems. Theoretical study of this model is rather limited. The only work beyond the molecular-field approximation (MFA) is a study of essentially the collective excitations in the random phase approximation.[6,13] No other physical quantities, including the critical temperature and zero-temperature magnetic moment, have been calculated beyond the MFA.

In this pair of papers (see following paper in this issue) we first devote ourselves to obtain an accurate estimate of the critical temperature for the singlet-triplet model, employing a high-temperature series expansion technique developed by Wang and Lee[14] for complicated level systems. This is the first attempt to compute accurately the critical temperature for the real magnetic systems with cubic crystal-field potentials such as fcc Pr, Pr_3Tl, and TbSb. To allow a discussion of the most interesting behavior observed in Pr_3Tl with small La dilution[11] and in the pure Pr_3Tl under hydrostatic pressure[15] most recently reported, a calculation of the ground-state magnetic moment in addition to the critical temperature is required. We shall discuss the results of the ground-state moment calculation using the constant coupling approximation in the second paper. A discussion of the behavior of the ground-state moment and that of the critical temperature near the onset of an induced-moment magnetism will also be presented and the relationship of these two physical quantities shown.

The calculation on the singlet-triplet model is extremely valuable in the understanding of the behavior of the induced-moment systems mentioned above. For example, a dilemma with the molecular-field theory is the inability to fit both the zero-temperature moment and the critical temperature of Pr_3Tl simultaneously with one exchange parameter. Furthermore, the molecular-field theory fails *entirely* in describing the zero-temperature moment versus critical-temperature behavior of Pr_3Tl diluted with the nonmagnetic La,[11] or placed under hydrostatic pressure[15] (which also changes the crystal-field to the exchange-interaction ratio). Our singlet-triplet model calculation shows that the discrepancies between the molecular-field theory predictions and the experimental observations come about simply because of the failure of the molecular-field theory to take account of (i) the correlations of fluctuations in calculating the critical temperature, and (ii) the zero-point quantum fluctuations in calculating the zero-temperature moment. They can not be construed as evidence of any inadequacy of the original Hamiltonian used to describe these systems.

It should also be mentioned that the technique developed in this work for the singlet-triplet model can be readily applied to other systems such as the $J=2, \frac{5}{2}$ magnetic systems in cubic fields, or generalized to treat the nine-energy-level Pr^{3+} problem. While the basic theory of the high-temperature series expansion has been given by Wang and Lee,[14] a major effort in this work is to develop computer algorithms for computing the large number of terms.

We have obtained the first five coefficients in the high-temperature series for the free energy and for the susceptibility. Each coefficient is a function of $\beta\Delta$, where Δ is the crystal-field energy gap between the singlet and the triplet and $\beta = 1/k_B T$. Namely, the susceptibility series is of the form

$$k_B T \chi = \sum_n a_n(\beta\Delta)[\beta\mathcal{J}(0)]^n \ , \tag{1}$$

where $\mathcal{J}(0)$ is the exchange-interaction parameter. We emphasize that the expansion is for an arbitrary crystal-field strength. It also allows for an arbitrary range of exchange interactions and lattice geometry.

We have used the standard ratio test technique to estimate the critical-temperatures T_c. Explicit results are given for the three cubic lattices with nearest-neighbor-only exchange interactions. We find that for all three lattices, the uncertainties in our estimated T_c are, in general, less than 4% and for the fcc, the appropriate lattice for the induced-moment compounds mentioned above, the uncertainty is less than 1%! The MFA results are also shown for comparison. We point out the total inadequacy of using the MFA in the discussion of experimental results for an induced-moment system with $\Delta/\mathcal{J}$ ratio close to the critical value for magnetic ordering, and that Pr_3Tl is just such a system.

In Sec. II, procedures for obtaining the high-temperature series expansion will be given. The use of a computer to evaluate the large number of terms will be discussed. We have broken Sec. II into four parts for easy reading. Section III is the conclusion. There we shall discuss the application of the singlet-triplet model results to the induced-moment compound Pr_3Tl.

II. HIGH-TEMPERATURE SERIES EXPANSION

A. Formulation

We describe the induced-moment singlet-triplet model in the context of a rare-earth system. The Hamiltonian is

$$\mathcal{H} = \sum_i V_{ci} - \sum_{ij} \mathcal{J}_{ij} \vec{J}_i \cdot \vec{J}_j - g_J \mu_B h \sum_i J_i^z \ , \tag{2}$$

where V_{ci} is the single-ion crystal-field potential which gives a singlet ground state and a set of triply degenerate excited states, separated by an energy gap Δ. We assume that all other excited states are so far remote in energy from this singlet-triplet manifold that they can be ignored in our calculations. It is also essential that there exists a nonvanishing matrix element of $\vec{J}$ between the ground state and one of the

states in the triplet in order to allow for the induced moment to occur. The second term in the Hamiltonian describes the exchange interactions between the ions. While the high-temperature series expansion (HTSE) formulation described below allows for anisotropic Heisenberg exchange interactions, we shall only give results for the case of isotropic exchange interactions. We consider the situation of a simple ferromagnetic ordering, such as that occurring in Pr_3Tl. We choose the z axis along the direction of ordering, and the last term in the Hamiltonian shows the Zeeman energy for an external-field h applied in that direction.

For definiteness, we consider the Pr^{3+} ions in a cubic crystal field. The ground-state $|0\rangle_c$ and the excited triplet states $|1\rangle_c$, $|2\rangle_c$, $|3\rangle_c$ for each ion are given[16] as linear combinations of eigenstates of J^z, i.e.,

$$|0_c\rangle = \left(\frac{5}{24}\right)^{1/2}(|4\} + |-4\}) + \left(\frac{7}{12}\right)^{1/2}|0\} \ , \tag{3}$$

$$|1_c\rangle = 2^{-1/2}(|4\} - |-4\}) \ , \tag{4}$$

$$|2_c\rangle = 8^{-1/2}(|-3\} + 7^{1/2}|1\}) \ , \tag{5}$$

$$|3_c\rangle = 8^{-1/2}(|3\} + 7^{1/2}|-1\}) \ , \tag{6}$$

where $|n\}$ denotes the eigenstate of J^z with $J^z = n$.

It is seen that we have $\langle 0_c|\vec{J}|0_c\rangle = 0$, so the crystal-field ground state is nonmagnetic. However, the off-diagonal matrix element $\langle 0_c|J^z|1_c\rangle = (\frac{20}{3})^{1/2}$ can mix the crystal-field eigenstates through an exchange field and thus allow moments to occur. In the molecular-field approximation the exchange Hamiltonian is reduced to a sum of single-ion potentials $-2\mathcal{J}(0)\langle J^z\rangle \sum_i J_i^z$, and $\langle J^z\rangle$ is then self-consistently obtained. [Here, $\mathcal{J}(0)$ is the sum over i of the exchange integral $\mathcal{J}_{ij}$.] for $\Delta/\mathcal{J}$ less than the critical value, the system is found to undergo a second-order phase transition as temperature is raised and reaches the critical-temperature T_c, at which $\langle J^z\rangle$ drops to zero continuously.[1] The molecular-field value of T_c is, however, too high.

In the high-temperature series expansion calculation which treats the single-ion potential exactly,[14] we first split the Hamiltonian into two parts. The single-ion Hamiltonian $\mathcal{H}_0$ consists of the crystal-field potential and the self-consistent molecular-field Hamiltonian; the perturbation part $\mathcal{H}_1$ describes the correlations of the fluctuations

$$\mathcal{H}_0 = \sum V_{ci} - [2\mathcal{J}(0)\langle J^z\rangle + g\mu_B h]J_i^z + \mathcal{J}(0)\langle J^z\rangle^2 \tag{7}$$

and

$$\mathcal{H}_1 = -\sum_{ij}\mathcal{J}_{ij}[J_i^+ J_j^- + (J_i^z - \langle J^z\rangle)(J_j^z - \langle J^z\rangle)] \ . \tag{8}$$

$\mathcal{H}_0$ can be solved exactly. The molecular-field eigenstates are then used as a basis to construct the HTSE for $\mathcal{H}_1$. We obtain the molecular-field eigenstates

$$|0\rangle = \cos\theta\,|0_c\rangle + \sin\theta\,|1_c\rangle \ , \tag{9}$$

$$|1\rangle = -\sin\theta\,|0_c\rangle + \cos\theta\,|1_c\rangle \ , \tag{10}$$

$$|2\rangle = |2_c\rangle \ , \tag{11}$$

and

$$|3\rangle = |3_c\rangle \ , \tag{12}$$

where

$$\tan 2\theta = 2\alpha h_m/\Delta \tag{13}$$

and

$$\alpha = \langle 0_c|J^z|1_c\rangle = \langle 1_c|J^z|0_c\rangle = (\tfrac{20}{3})^{1/2}$$

for Pr^{3+} in a cubic field. The molecular-field eigenenergies are

$$\epsilon_0 = \frac{\Delta}{2}\left\{1 - \left[1 + \left(\frac{2\alpha h_m}{\Delta}\right)^2\right]^{1/2}\right\} \ , \tag{14}$$

$$\epsilon_1 = \frac{\Delta}{2}\left\{1 + \left[1 + \left(\frac{2\alpha h_m}{\Delta}\right)^2\right]^{1/2}\right\} \ , \tag{15}$$

$$\epsilon_2 = \Delta - 0.5h_m \ , \tag{16}$$

$$\epsilon_3 = \Delta + 0.5h_m \ , \tag{17}$$

where

$$h_m = g\mu_B h + 2\mathcal{J}(0)\langle J^z\rangle \ . \tag{18}$$

The molecular-field free energy per ion F_0 is thus given by

$$-\beta F_0 = \ln \sum_{n=0}^{3} \exp(-\beta\epsilon_n) - \beta\mathcal{J}(0)\langle J^z\rangle^2 \ . \tag{19}$$

The corrections to F_0 can be obtained by using the standard finite-temperature perturbation theory for the many-body systems.[17]

$$-\beta\Delta F = \sum_{n=1}^{\infty}\frac{(-1)^n}{n!}\int_0^\beta d\tau_1 \cdots \int_0^\beta d\tau_n \langle T_\tau \mathcal{H}_1(\tau_1)\mathcal{H}_1(\tau_2)\cdots\mathcal{H}_1(\tau_n)\rangle_c \ , \tag{20}$$

where $\mathcal{H}_1$ has been written in the interaction representation with $\mathcal{H}_0$ as the unperturbed Hamiltonian. The angular brackets denote the canonical thermal average over $\mathcal{H}_0$. The subscript c denotes the cumulant part of the τ-ordered product, or, in the diagrammatic analysis, the contribution of only the connected diagrams. Equations (19) and (20) consist of a HTSE of the free energy in powers of $\beta\mathcal{J}$, from which other thermodynamic quantities can be obtained. For example, the susceptibility is the negative of the second derivative of F with respect to the external field.

B. Diagrammatic technique

To compute ΔF we need a method to evaluate the thermal averages of the τ-ordered products of angular momentum operators. A Wick-like theorem which enables one to evaluate the product as a sum of products of pairs—the unperturbed Green's functions—is highly desirable because it permits a diagrammatic representation of the perturbation series and facilitates the computation. The method of Vaks, Larkin, and Pikin[18] is however, not applicable, because the inclusion of the crystal-field potential in the unperturbed Hamiltonian $\mathcal{H}_0$ destroys the simple τ dependence of the angular momentum operators in the interaction representation. A more general scheme has been furnished by Yang and Wang[19] recently. They employed the standard basis operator[20] $L_{mn} \equiv |m\rangle\langle n|$, which transfers an ion from the nth state to the mth state, in their formulation. (We shall also call these operators L operators in later reference.) Because of the simple τ dependence of the operator $L_{mn}(\tau)$ in the interaction representation a Wick-like theorem can be derived. A diagrammatic representation of the terms in the perturbation expansion has been developed.[19] A price one has to pay, however, is the effort in handling a greater number of operators. A computer is, therefore, extremely valuable in this regard.

A diagram can be constructed with the "semi-invariants" $\langle T_\tau J_l^\alpha J_l^\beta \cdots \rangle_c$ and the exchange-interaction lines connecting $J_l^z J_j^z$, or $J_l^\pm J_j^\mp$. Diagrams so obtained will be called the main diagrams. For the singlet-triplet model studied here there are two second-order, four third-order, and eleven fourth-order main diagrams. These are shown in Fig. 1 where the semi-invariant $\langle T_\tau J_i^\alpha J_l^\beta \cdots J_i^\delta \rangle_c$ is represented by an oval.

As discussed earlier, the semi-invariants (hereafter, abbreviated as SI) are evaluated in the standard basis operator representation. As a result, each SI in the angular momentum operators is equal to a sum of SI's in the standard basis operators. In our model we have

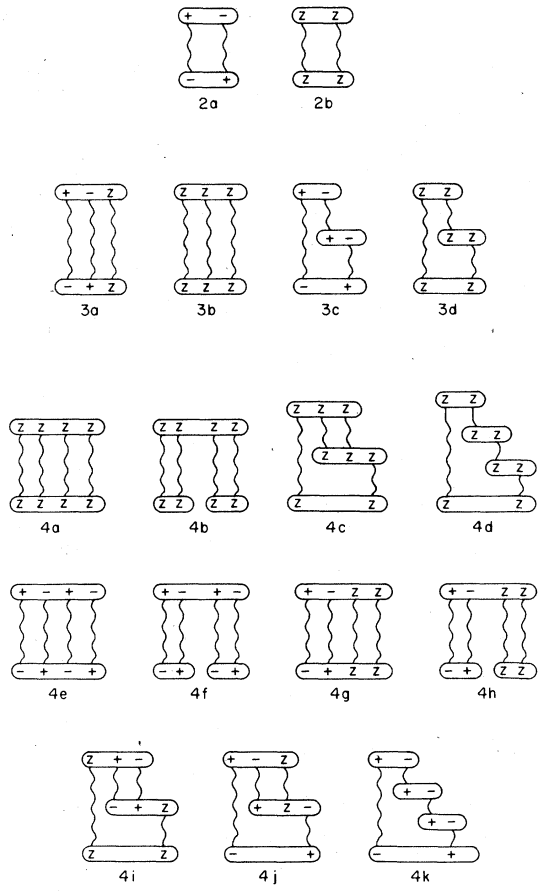

FIG. 1. Free energy "main diagrams" for the singlet-triplet model (Pr^{3+} in a cubic field). Each oval represents a semi-invariant. J^α is denoted by α and the wavy lines represent the exchange interactions.

$$J^z = A_{01}(L_{10}+L_{01}) + A_{00}(L_{00}-L_{11}) + A_{22}(L_{22}-L_{33}) \ , \tag{21}$$

$$J^+ = A_{02}L_{20} + A_{12}L_{21} + A_{03}L_{03} + A_{13}L_{13} \ , \tag{22}$$

$$J^- = A_{02}L_{02} + A_{12}L_{12} + A_{03}L_{30} + A_{13}L_{31} \ , \tag{23}$$

where the matrix elements are

$$A_{01} = \alpha\cos 2\theta, \quad A_{00} = \alpha\sin 2\theta, \quad A_{22} = 0.5 \ ,$$

$$A_{02} = 2^{1/2}(\alpha\cos\theta - 0.5\sin\theta) \ ,$$

$$A_{12} = -2^{1/2}(\alpha\sin\theta + 0.5\cos\theta) \ ,$$

$$A_{03} = 2^{1/2}(\alpha\cos\theta + 0.5\sin\theta) \ ,$$

$$A_{13} = 2^{1/2}(0.5\cos\theta - \alpha\sin\theta) \ .$$

To illustrate the evaluation of an SI, we calculate $\langle T_\tau J^+(\tau) J^-(0)\rangle_c$. We obtain

$$\langle T_\tau J^+(\tau) J^-(0)\rangle_c = -A^2_{02}D_{02}G^0_{02}(\tau) - A^2_{12}D_{12}G^0_{12}(\tau) + A^2_{03}D_{03}G^0_{30}(\tau) + A^2_{13}D_{13}G^0_{31}(\tau) \ , \tag{24}$$

where we have evaluated each SI in the L operators in terms of the Green's functions, i.e.,

$$\langle T_\tau L_{mn}(\tau) L_{nm}(0)\rangle_c = D_{mn}G^0_{nm}(\tau) \equiv \begin{cases} D_m e^{\epsilon_{mn}\tau}, & \tau > 0 \\ D_n e^{\epsilon_{mn}\tau}, & \tau < 0 \end{cases} \tag{25}$$

where

$$\epsilon_{mn} = \epsilon_m - \epsilon_n \ , \quad D_{mn} = D_m - D_n$$

and

$$D_m = e^{-\beta\epsilon_m} / \sum_n e^{-\beta\epsilon_n} \ .$$

We can represent each Green's function $G^0_{nm}(\tau)$ by a line labeled by (nm) propagating from 0 to τ. D_{mn} is a weight factor associated with the SI $\langle T_\tau L_{mn}(\tau) L_{nm}(0)\rangle_c$. Therefore, the SI $\langle T_\tau J^+(\tau) J^-(0)\rangle_c$ consists of four SI's in L operators, each of which is a Green's function with a weight factor. Appropriate matrix elements, which occur in expressing the angular momentum operators in terms of the L operators, should also be multiplied to each SI of the L operators to reconstruct the original SI in the angular momentum operators.

As discussed in Ref. (19), the diagrammatic representation need not be unique and in fact is not unique for an SI in the angular momentum operators, nor is it unique for an SI in the L operators. The final results are, of course, equal. The difference in the appearance of the results is caused by adopting a different operator to pair with the other operators in the Wick reduction process. More details are given in Ref. (19). In this paper, we have adopted the priority order for the operators in engaging such pairing-reduction process in the order of L_{02}, L_{12}, L_{30}, L_{31}. These operators all belong to the angular momentum operator J^-. In the higher-order cases, L_{02} may pair with L_{30} and the corresponding commutator produces L_{32}, which belongs to $(J^-)^2$. We assign to such operators a higher priority over the J^- operators. If there is more than one L operator of $(J^-)^2$ present, we assign a higher priority to the L_{mn} with the smallest value of m, and if two operators have the same value of m, then the one with smaller value of n is assigned the higher priority. In the presence of J^z, we take L_{01} to be "active" but assign a lower priority to this operator in competition with the operators of $(J^-)^2$ and J^-.

It is clear that a two point SI gives a single Green's function or a pair of isolated points, the latter being the case with the diagonal operators L_{nn}; e.g., $\langle T_\tau L_{nn}(\tau) L_{mm}(0)\rangle_c$, which is equal to $D_n\delta_{mn} - D_nD_m$, is represented by two points labeled m and n and circled in an oval. The more general case of n operators can have terms consisting of up to $n-1$ Green's functions; the diagonal operators can either be isolated points, as just shown, or scattering vertices. In the latter case, a Green's function will not change its identity after scattering but may change the frequency it carries. This occurs in the three point SI

$$\langle T_\tau L_{20}(\tau_1) L_{02}(\tau_2) L_{22}(\tau_3)\rangle_c \ ,$$

which consists of two terms after the Wick reduction, as shown in Fig. 2(a) and 2(b); in Fig. 2(a) L_{22} has not participated in the Wick reduction process but in Fig. 2(b) it is a scattering vertex. In general, an SI with more than two operators is represented by a sum of more than one graph. Each graph shall be called a sub-SI. For example, the two sub SI's of

$$\langle T_\tau L_{20}(\tau_1) L_{02}(\tau_2) L_{22}(\tau_3)\rangle_c$$

are shown in Fig. 2(a) and 2(b). The weight factors associated with the two sub-SI's are $D_2 + D_2D_{02}$ and D_{02}, respectively. They can be simply obtained by applying the Wick reduction procedure to the τ-ordered product until no operator except the diagonal ones remains, then, taking the cumulant part of the product as described by Yang and Wang.[19]

The sub-SI's are the fundamental building blocks for the more fundamental diagrams, the subdiagrams—as we shall call them—to be distinguished from the main-diagrams defined earlier. A main diagram in general is composed of a set of subdiagrams. For example, the second-order transverse diagram Fig. 1 (2a) contains ten subdiagrams as shown in Fig. 3(a) where the Green's function lines can be either G^0_{02}, G^0_{30}, G^0_{12}, or G^0_{31}. For the second-order longitudinal diagram Fig. 1(2b), a total of four different subdiagrams are obtained. They are shown in Fig. 3(b), 3(c), and 3(d). Here the Green's function line can only be G^0_{01} but can point in either direction. The number of subdiagrams multiplies quickly as we go on to higher orders. For example, if we consider the main diagram shown in Fig. 1 (4e), there are 34 different sub-SI's. A subdiagram can be constructed by using any two of such pieces (which can be identical). Therefore, we obtain a total of 595 subdiagrams. There are, however, only 12 different irreducible general structures for the diagrams. These are shown in Fig. 4. For convenience of drawing, we have shrunk each interaction line to a point in the diagram. A definition of general structure is in

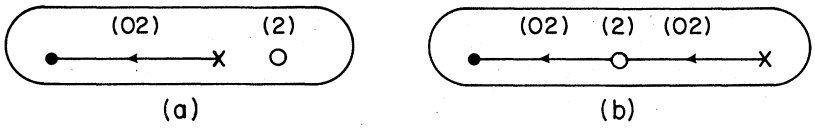

FIG. 2. Sub-semi-invariants of $\langle T_\tau L_{20}(\tau_1) L_{02}(\tau_2) L_{22}(\tau_3)\rangle_c$. (a) shows an isolated diagonal vertex and (b) shows a scattering diagonal vertex.

order. Two diagrams are said to have the same general structure if one can be reduced to the other after omitting the energy arguments and the propagating direction of all the Green's functions in the two diagrams. An irreducible general structure is a general structure which can not be separated into two general structures by slicing through a point. The introduction of the irreducible general structure facilitates the calculation of the diagrams as will be shown in the Sec. II C.

C. Evaluation of diagrams

Each subdiagram is evaluated in the Fourier space. In the Fourier space each Green's function carries a frequency $\omega_l = 2l\pi k_B T$ (l being an integer), and contributes a factor

$$G^0_{mn}(\omega_l) = -k_B T(i\omega_l - \epsilon_{mn})^{-1} \ ,$$

which is the Fourier transform of $G^0_{mn}(\tau)$. Each interaction line carries a wave-vector $\vec{q}$ and contributes a factor $\beta\mathcal{J}(\vec{q})$. The sum of frequencies at each vertex of interaction is conserved, so is the sum of wave vectors at each sub-SI site of a diagram. The evaluation of a diagram involves summations over the frequemcy and wave-vector variables. The former can be accomplished by using Poisson's summation formula, while the latter depends on the geometry of the lattice as well as the range of interactions.

As mentioned earlier in this section, the number of subdiagrams has already become enormous even up to the fourth order. A computer is indeed necessary to assist in doing the bookkeeping and even in the actual evaluations of the diagrams. We have written a subroutine which produces analytic expressions of a function $f(\epsilon_1, \epsilon_2, \epsilon_3, \ldots, \epsilon_n)$ for cases of two or more of the parameters ϵ_n being equal. For example

$$f(\epsilon_1, \epsilon_2) = [n(\epsilon_1) - n(\epsilon_2)]/(\epsilon_1 - \epsilon_2) \ ,$$

where $n(\epsilon)$ is a Bose factor with energy ϵ. The subroutine yields $n'(\epsilon_1)$ for an input of $\epsilon_1 = \epsilon_2$; it replaces ϵ_2 by $\epsilon_1 + \delta$, expands each quantity in powers of δ and obtains the limit at $\delta \to 0$. With the help of this subroutine, we only need to provide analytic results for a small number of frequency sums, one for each irreducible general structure. They are calculated with all energies of Green's functions being different. Up to the 4th order, the irreducible general structures

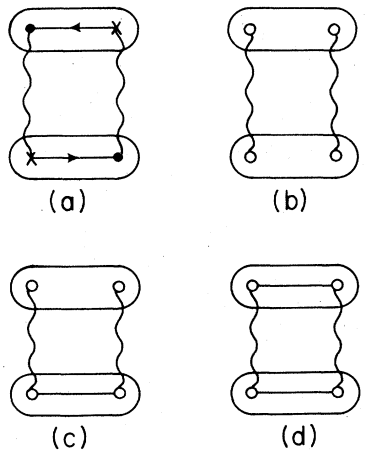

FIG. 3. Subdiagrams of the main diagrams 1(2a), 1(2b). (a) gives ten different diagrams when the labels of the Green's functions are shown. In (c) and (d) the Green's function lines are G^0_{01} but can propagate in either direction.

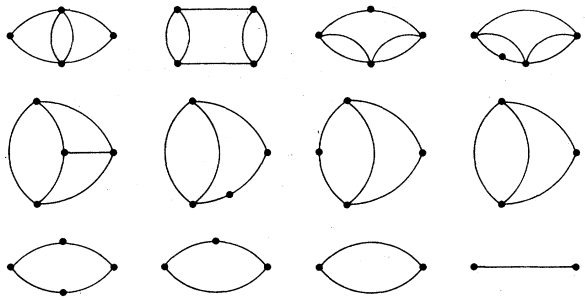

FIG. 4. Irreducible general structures. These are the ones for which frequency sums are calculated manually. They are used as inputs for the computer calculations of frequency sums of all diagrams up to the fourth order.

shown in Fig. 4 are the only ones which appear, although the total number of different diagrams when the arguments of the Green's functions are put back exceeds 3000. The computer generates analytic results for each subdiagram and stores them in a file. The result of the frequency sum of each subdiagram is then multiplied by the weight factors of the sub-SI's which have been used to construct the diagram. A counting factor is also multiplied to each subdiagram. The counting factor for an nth-order diagram is $P/n!$, P being the number of topologically distinct diagrams obtainable by permuting the indices of the diagram. Finally, the result is multiplied to the wave-vector sum, a lattice sum, which depends only on the main diagram to which the subdiagram belongs.

The contribution of a main diagram is the sum of the subdiagram properly weighted by the matrix elements, which occurred when the standard basis representation was used for each angular momentum operator as shown in Eqs. (21) – (23). The final result of a diagram is a function of a set of basic quantities, D_α, ϵ_α, derivatives of D_α, and the matrix elements A_{mn}. The function is extremely complex and lengthy. To compute the susceptibility, the second derivative of this function with respect to the external field evaluated in the zero-field limit is required. To make the calculation feasible, we expand from the outset, each basic quantity, involved in the later calculations, in a power series of h_m. It has been found necessary to keep terms in each power series up to the eighth power, because in the process of calculation, quantities in h_m^{-6} may occur. It is a simple matter for a computer to perform the addition or multiplication of two power series. The total number of operations, though manageable by a computer, is enormous. We also note that in this procedure the computation is carried out for each fixed value of $\beta\Delta$, starting each time from the basic quantities. As will be shown later, in the determination of T_c, it is the value of $\Delta/\mathcal{J}$ we hold fixed, and values of a diagram for a continuous spectrum of values of $\beta\Delta$ are needed for such purpose. The precedure above is too costly for computing for a large number of points.

It is possible, however, to obtain the free energy in power series of h_m with coefficients as functions of $\beta\Delta$ analytically. We represent each basic quantity in the form

$$\sum_{m,n} b_{mn}(\beta\Delta)^{-m}t^n(1+3t)^{-r}(1-t)^{-s} ,$$

with $t=\exp(-\beta\Delta)$. r and s are a set of fixed numbers for each basic quantity, and m, n vary from zero to some finite numbers. b_{mn} is then a two-dimensional array. But noticing that the whole expression here is a coefficient in the power series of h_m, b_{mn} is in fact a three-dimensional array $b_{mn}^{(p)}$, where p is the power of h_m in the series. An analytic expression for the coefficients in the power series of h_m for the free energy can be written

$$(1+3t)^{-r}\sum_{m,n} C_{mn}(\beta\Delta)^{-m}t^n .$$

Here, again r is a fixed number. The denominator $(1-t)^s$ which appears in the basic quantities has been canceled by factors in the t series in the numerator.

We present the results of such calculation in Table II. We only show the second derivative of the free energy contribution with respect to h_m at $h_m=0$. The magnetic susceptibility is related to this derivative in a simple way. We have

$$\chi=\frac{\chi_c}{1-2\mathcal{J}(0)\chi_c} , \tag{26}$$

with

$$\chi_c=-\frac{\partial^2 F}{\partial h_m^2} . \tag{27}$$

In Table I we have grouped the diagrams of a common lattice sum (wave-vector sum) together,[21] and we have only carried out such calculation to the third order. The fourth-order calculation with the three-dimensional arrays would take a large memory space in the computer. Since we had planned to stop at the fourth order, only a finite number of points at this order with fixed values of $\beta\Delta$ are needed (instead of a continuous spectrum) for the estimation of T_c. We have computed the fourth-order terms numerically for a selection of values of $\beta\Delta$. The results are shown in Table II where again only terms for χ_c are presented and diagrams of a common lattice sum are grouped.

D. Series analysis and determination of T_c

We have obtained five terms in the HTSE of the susceptibility. The first two terms can be found from the MFA, the other three terms are obtained as discussed above. The result is valid for arbitrary values of $\Delta/\mathcal{J}$ ratio, that is for an arbitrary strength of the crystal-field potential. The series is also for a general lattice and a general exchange interaction, since the lattice sums are computed separately.

Using the data in Tables I and II we construct the power series of χ_c,

$$k_B T\chi_c=\sum_n C_n(\beta\Delta)[\beta\mathcal{J}(0)]^n , \tag{28}$$

where

$$C_0=\frac{40(1-t)}{3(\beta\Delta)(1+3t)}+\frac{t}{2(1+3t)} , \tag{29}$$

$$C_2=b_{21}R_{21} , \tag{30}$$

$$C_3=b_{31}R_{31}+b_{32}R_{32} , \tag{31}$$

$$C_4 = b_{41}R_{41} + b_{42}R_{42} + b_{43}R_{43} + b_{44}R_{21}^2 \quad . \tag{32}$$

Here b_{21}, b_{31}, b_{32} are given in Table I and b_{41}, b_{42}, b_{43} in Table II. The lattice sums are

$$R_{21} = \frac{1}{N}\sum \frac{\mathcal{J}^2(\kappa)}{\mathcal{J}^2(0)} \quad , \tag{33}$$

$$R_{31} = \frac{1}{N}\sum \frac{\mathcal{J}^3(\kappa)}{\mathcal{J}^3(0)} \quad , \tag{34}$$

$$R_{32} = \frac{1}{N}\sum \frac{\mathcal{J}(\kappa_1)\mathcal{J}(\kappa_2)\mathcal{J}(\kappa_1+\kappa_2)}{\mathcal{J}^3(0)} \quad , \tag{35}$$

$$R_{41} = \frac{1}{N}\sum \frac{\mathcal{J}^4(\kappa)}{\mathcal{J}^4(0)} \quad , \tag{36}$$

$$R_{42} = \frac{1}{N^2}\sum \frac{\mathcal{J}(\kappa_1)\mathcal{J}(\kappa_2)\mathcal{J}^2(\kappa_1+\kappa_2)}{\mathcal{J}^4(0)} \quad , \tag{37}$$

$$R_{43} = \frac{1}{N^3}\sum \frac{\mathcal{J}(\kappa_1)\mathcal{J}(\kappa_2)\mathcal{J}(\kappa_3)\mathcal{J}(\kappa_1+\kappa_2+\kappa_3)}{\mathcal{J}^4(0)} \quad . \tag{38}$$

In the case of nearest-neighbor-only interaction, these sums reduce to, for the three cubic lattices (sc, bcc, fcc),

$$R_{21} = \tfrac{1}{6}, \tfrac{1}{8}, \tfrac{1}{12} \quad R_{31} = 0, 0, \tfrac{1}{36}$$

$$R_{32} = \tfrac{1}{36}, \tfrac{1}{64}, \tfrac{1}{144}$$

$$R_{41} = \tfrac{5}{72}, \tfrac{27}{512}, \tfrac{5}{192} \quad R_{42} = 0, 0, \tfrac{1}{432}$$

$$R_{43} = \tfrac{1}{216}, \tfrac{1}{512}, \tfrac{1}{1728} \quad .$$

It is a simple matter to relate the coefficients of the power series of χ_c and χ. We find

$$a_0 = C_0 \quad , \tag{39}$$

$$a_1 = 2C_0^2 \quad , \tag{40}$$

$$a_2 = 4C_0^3 + C_2 \quad , \tag{41}$$

$$a_3 = 8C_0^4 + 4C_0C_2 + C_3 \quad , \tag{42}$$

$$a_4 = 16C_0^5 + 12C_0^2C_2 + 4C_0C_3 + C_4 \quad . \tag{43}$$

The critical temperature is determined by the condition $\chi \to \infty$, that is when the series diverges. Applying the ratio test to the series, we locate the critical temperature. We have

$$\lim_{n\to\infty} \frac{a_n}{a_{n-1}} = \frac{k_B T_c}{\mathcal{J}(0)} \quad . \tag{44}$$

For a series with only a finite number of terms known, we can only estimate the value of T_c by extrapolation. We define

$$\frac{k_B T_c^{(n)}}{\mathcal{J}(0)} = \frac{a_n(\beta_c\Delta)}{a_{n-1}(\beta_c\Delta)} \quad . \tag{45}$$

With the first five terms known in our series, we can find $T_c^{(n)}$ for $n=1$ through 4 for a fixed value of $\Delta/\mathcal{J}(0)$ ratio. We note that $T_c^{(1)}$ is simply the critical temperature given by the MFA. If we plot $T_c^{(n)}$ vs $1/n$ we obtain four points. An estimate of T_c^{∞}, which is the critical temperature given by Eq. (44), can usually be obtained by an appropriate extrapolation. The

TABLE I. Coefficients used to construct C_2 and C_3, Eq. (30) and Eq. (31); $b_{\alpha\beta} = (1+3t)^{-r}\sum_{m,n} C_{mn}(\beta\Delta)^{-m} t^n$.

	m	r	C_{m0}	C_{m1}	C_{m2}	C_{m3}	C_{m4}
	0	3	0.0	44.444444444	−133.14583333	−0.6875000000	
b_{21}	1	3	0.0	−5222.9629630	13075.555556	233.33333333	
	2	3	0.0	−546.66666667	−28188.148148	0.0	
	3	3	−9570.3703704	35539.259259	−13632.592593	−12336.296296	
	0	4	0.0	197.53086420	−1580.2469136	−592.38425926	−0.6250000000
	1	4	0.0	−43917.695473	91315.349794	53555.802469	103.33333333
b_{31}	2	4	0.0	−262011.52263	−471624.60905	−821602.96296	−3831.8518519
	3	4	0.0	13339.917695	−128434.73251	130146.17284	−15051.358025
	4	4	−121744.85597	1422801.6461	−1892161.3169	2897.1193416	588207.40741
	0	4	0.0	0.0	−88.847222222	88.576388889	0.6875000000
	1	4	0.0	−88.888888889	24558.148148	−1827.4074074	−781.11111111
b_{32}	2	4	0.0	14907.777778	−1550367.5926	−679354.56790	3206.4814814
	3	4	0.0	1363651.1111	4283022.3457	−2480339.2593	−269688.27160
	4	4	180390.12346	−3470857.6543	2813504.3210	1167357.9012	−690394.69136

TABLE II. Coefficients used to construct C_4 [Eq. (32)] for a selection of values of $\beta\Delta$.

$\beta\Delta$	b_{41}	b_{42}	b_{43}	b_{44}
1.5	-2.61175×10^{4}	4.24365×10^{4}	-3.49116×10^{4}	9.35949×10^{4}
2.0	-2.46217×10^{4}	4.01603×10^{4}	-2.96218×10^{4}	8.87712×10^{4}
3.0	-1.29474×10^{4}	2.05162×10^{4}	-2.08060×10^{4}	4.62329×10^{4}
3.5	-8.02176×10^{3}	1.25018×10^{4}	-1.00535×10^{4}	2.86400×10^{4}
4.0	-4.74612×10^{3}	7.33068×10^{3}	-5.86927×10^{3}	1.71066×10^{4}
4.5	-2.76323×10^{3}	4.28010×10^{3}	-3.42775×10^{3}	1.01705×10^{4}
5.0	-1.61533×10^{3}	2.54254×10^{3}	-2.04466×10^{3}	6.13874×10^{3}
6.0	-5.85509×10^{2}	9.83965×10^{2}	-8.02531×10^{2}	2.42819×10^{3}
8.0	-1.09563×10^{2}	2.17524×10^{2}	-1.81614×10^{2}	5.43259×10^{2}
9.0	-5.63932×10^{1}	1.18867×10^{2}	-9.97884×10^{1}	2.96768×10^{2}
10.0	-3.17903×10^{1}	6.96539×10^{1}	-5.86405×10^{1}	1.73744×10^{2}

deviations of the points from being on a straight line provide a measure of the uncertainty in the value of T_c so obtained. Before we show such a plot, we should note that the coefficients of the power series are functions of $\beta\Delta$, thus T_c is most easily obtained from Eqs. (44) and (45) with a fixed value of $\beta\Delta$. We, however, are interested in T_c as a function of $\Delta/\mathcal{J}$. This goal can be achieved by solving Eq. (45) for $T_c^{(n)}/\mathcal{J}$ using the Newton-Raphson iteration method for a fixed value of $\Delta/\mathcal{J}$. The procedure, then, requires the values of the coefficients $a_n(\beta\Delta)$ known for all $\beta\Delta$, instead of a set of discrete values of the quantity as is the case with the fourth-order coefficients. To make use of the fourth-order coefficients, which are known only for a selective set of values of $\beta\Delta$, we first use Eq. (45) to obtain $T_c^{(4)}/\mathcal{J}$ for each value of $\beta\Delta$. We then multiply $T_c^{(4)}/\mathcal{J}$ to $\beta\Delta$ to find the corresponding value of $\Delta/\mathcal{J}$. With this value of $\Delta/\mathcal{J}$ fixed $T_c^{(n)}/\mathcal{J}$ for $n=1-3$ can be found by the Newton-Raphson method.

We have obtained $T_c^{(n)}$ ($n=1$ to 4) for an fcc lattice with nearest-neighbor-only exchange interaction, and found that the points of $T_c^{(n)}$, except the first one (MFA), all lie very well on a straight line in the $1/n$ plot. Several representative cases are shown in Fig. 5. We note that there is a small deviation of the points from a straight line as the critical value of $\Delta/\mathcal{J}$ ratio is approached. Generally speaking a straight line can be drawn through the points after ignoring $T_c^{(1)}$. Happily, this is the case relevant to Pr_3Tl and fcc Pr, where the Pr^{3+} ions are situated in an fcc lattice.

The critical temperatures estimated by extrapolating the straight line, joining $T_c^{(2)}$ and $T_c^{(3)}$, to the $1/n=0$ axis are shown as a continuous curve in the plot of k_BT_c vs Δ in Fig. 6. Both k_BT_c and Δ are measured in the unit of $\mathcal{J}(0)\alpha^2$. The extrapolation of the line joining $T_c^{(2)}$ and $T_c^{(4)}$ locates the critical temperatures shown in the closed circles. Because the fourth-order coefficients are known for a finite number of $\beta\Delta$ values, a curve can not be constructed. We also note that generally in the $T_c^{(n)}$ vs $1/n$ plot, $T_c(n)$ oscillate about the straight line through the points of high orders (i.e., for large n); the deviation of $T_c^{(n)}$ from the straight line becomes smaller as n increases. Therefore, an extrapolation of the straight line joining $T_c^{(2)}$ and $T_c^{(4)}$ is believed to give a better estimation than by extrapolating the line joining $T_c^{(3)}$ and $T_c^{(4)}$. For an fcc lattice the difference is very minute as expected from the fact that $T_c^{(2)}$, $T_c^{(3)}$, and $T_c^{(4)}$ are almost on a straight line. That this is indeed the case is shown in Fig. 6, where the $T_c^{(2)}-T_c^{(4)}$ points (closed circles) deviate from the $T_c^{(2)}-T_c^{(3)}$ curve by less

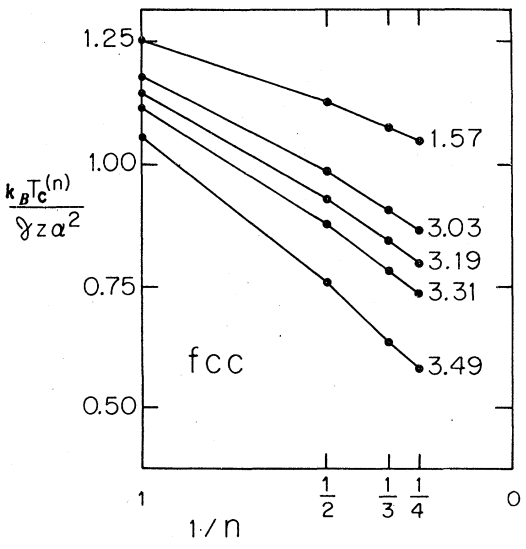

FIG. 5. $T_c^{(n)}$ vs $1/n$ plot for an fcc lattice. Each curve is labeled by the value of $\Delta/\mathcal{J}z\alpha^2$.

than 1%. While it is difficult to measure the uncertainty in the extrapolated value from a short series, based on the general behavior observed in the long series expansion for the simple Heisenberg and Ising systems we estimate the uncertainty involved in our estimated T_c to be about 1%. The MFA prediction is also plotted in Fig. 6 for comparison. A gross overestimation in the MFA is not unexpected.

We also present results for the simple cubic and body-center cubic lattices with nearest-neighbor-only exchange interaction. The $T_c^{(n)}$ vs $1/n$ plot for each of the lattices shows the familiar oscillation behavior. Some representative cases are shown in Figs. 7 and 8. The estimated values of T_c as a function of Δ are shown in Fig. 9 for sc and in Fig. 10 for bcc. The HTSE curve in each figure is obtained by an extrapolation of the line joining $T_c^{(2)}$ and $T_c^{(3)}$, and the closed circles by the line joining $T_c^{(2)}$ and $T_c^{(4)}$. The values from the two estimates can differ by 4% because of this oscillatory behavior of $T_c^{(n)}$. The estimates from the $T_c^{(2)} - T_c^{(4)}$ line should be more accurate and the uncertainty in the values should be about 4%.

III. CONCLUSION

As discussed in Sec. I, the motivation of this work is to develop an accurate method for computing the critical temperatures of the induced moment systems such as Pr_3Tl, fcc Pr, and TbSb. The circumstance is that experimental measurements have achieved such a high accuracy that the MFA—the only theory which has been applied to such systems—has become totally inadequate. As a first attempt to solve the whole problem, we focus our attention on the singlet-triplet model which has been used as a simplified version to describe these systems. We have obtained five terms in the HTSE for the free energy and for the susceptibility. The results are for an arbitrary lattice and range of interaction, and are valid for an arbitrary strength of the crystal-field potential. The critical temperatures are estimated for the nearest-neighbor-interaction model for the three cubic lattices. The fcc lattice calculation, which is appropriate for the induced-moment compounds mentioned above, shows that the estimated values

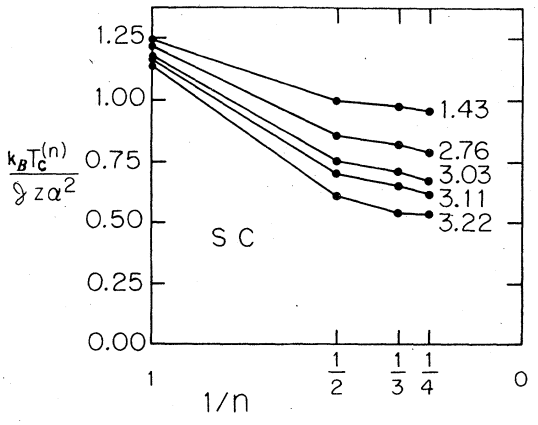

FIG. 7. $T_c^{(n)}$ vs $1/n$ plot for an sc lattice. Each curve is labeled by the value of $\Delta/\mathcal{J}z\alpha^2$.

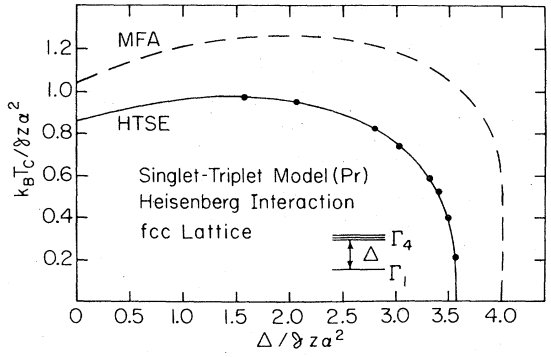

FIG. 6. Variation of the critical temperature with the crystal-field to the exchange-interaction ratio for a nearest-neighbor interaction model with an fcc lattice. The solid line is an estimate from the extrapolation of the line joining $T_c^{(2)}$ and $T_c^{(3)}$. The solid circles are estimates from the $T_c^{(2)} - T_c^{(4)}$ extrapolations, which are the most accurate estimates that we can obtain in this calculation. The dashed line shows the MFA values.

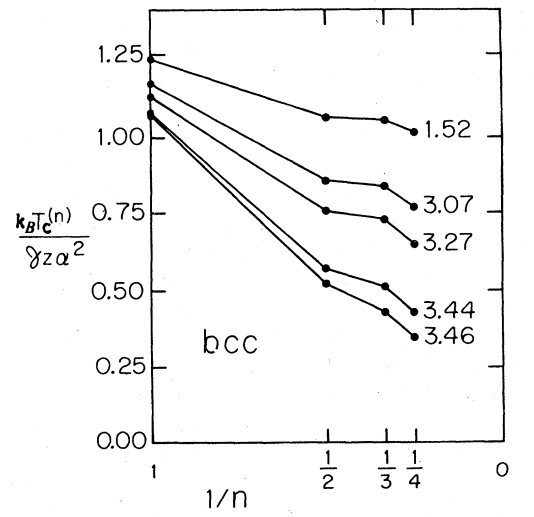

FIG. 8. $T_c^{(n)}$ vs $1/n$ plot for a bcc lattice. Each curve is labeled by the value of $\Delta/\mathcal{J}z\alpha^2$.

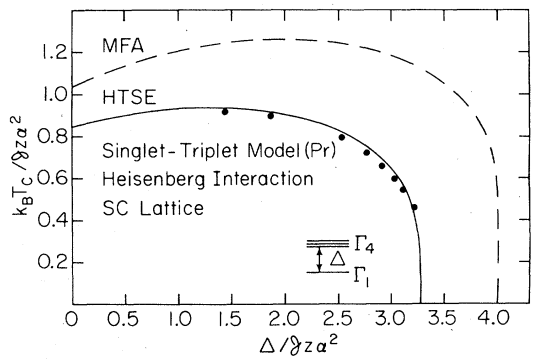

FIG. 9. Same as Fig. 6 but for an sc lattice. Very close to the critical value for ordering the $T_c^{(2)} - T_c^{(4)}$ extrapolation shows anomalous behavior. These few points have been dropped from the figure.

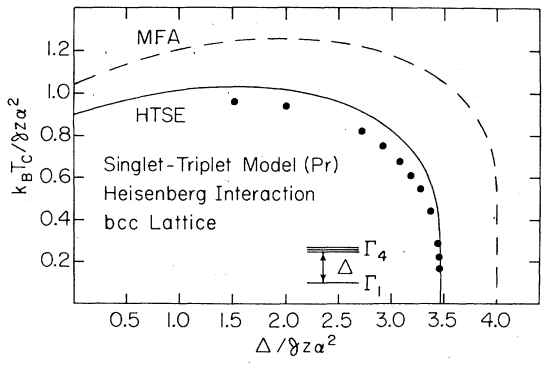

FIG. 10. Same as Fig. 6 but for a bcc lattice.

for T_c should be within 1% from the exact values. This is to be compared with the MFA result which is only qualitatively correct.

It is of interest to deduce the exchange-interaction parameter from the measured values of the crystal-field energy splitting Δ (between the singlet and the triplet) and the critical temperature T_c. This can be simply done in Fig. 6, where $T_c/\mathcal{J}$ is shown to vary with $\Delta/\mathcal{J}$. We first locate a point $(1, T_c/\Delta)$ on the figure, the intercept of the straight line, drawn from the origin to this point, with the curve then allows us to determine the value of $\mathcal{J}z\alpha^2$ (where $\alpha^2 = 20/3$ and $z = 12$). We recall that the curve was calculated for Pr^{3+} and is applicable to the cubic Pr compounds only. For Pr_3Tl, $\Delta = 77$ °K and $T_c = 12$ °K, we find that $\mathcal{J} = 0.28$ °K. The MFA value for $\mathcal{J}$ is 0.24 °K and is about 15% too low. On the other hand, taking the correct value of $\mathcal{J} = 0.28$ °K, MFA predicts $T_c = 25$ °K which is twice the actual T_c! This is because the value of $\Delta/\mathcal{J}$ for Pr_3Tl is quite close to the critical value ($\Delta/\mathcal{J}$ being 0.95 times the critical value). We should recall that the above analysis is based on the singlet-triplet model, and the higher-lying excited states may have non-negligible effect as seen in the MFA analysis.[22] It is also important to note that Pr_3Tl unlike fcc Pr has actually a more complicated structure. In fact, each Pr ion has four Tl nearest neighbors and eight Pr nearest neighbors arranged as on an fcc lattice. The neutron work on the powdered samples does not yield full information for the range of the exchange interaction which presumably extends to second and third nearest neighbors or farther. Due to the lack of detailed information about $\mathcal{J}(q)$, we have chosen the fcc nearest-neighbor interaction model in our discussion. An important point we wish to make here is that for systems, like Pr_3Tl, with the $\Delta/\mathcal{J}$ ratio close to the critical value, T_c calculated in the MFA (with $\mathcal{J}$ determined in other measurements) can be off by a tremendous amount when compared to the measured value.

To determine the ratio $\Delta/\mathcal{J}$ of an induced-moment system, one can also resort to the measurements of the low-temperature moment (extrapolating to zero temperature). The ground-state moment can be simply calculated in the MFA. However, the effects of zero-point fluctuations are entirely ignored in the approximation and the validity of the result is in serious doubt, especially for values of $\Delta/\mathcal{J}$ close to the critical value for ordering as in the case of Pr_3Tl. It is therefore important to perform a more accurate calculation for the ground-state moment in order to discuss the behavior of Pr_3Tl, or other systems with the $\Delta/\mathcal{J}$ ratio close to the critical value. This will be the subject of the second paper which follows. We also postpone our discussion of the behavior observed in Pr_3Tl diluted with La and that in Pr_3Tl under a hydrostatic pressure until a more accurate ground-state moment is obtained in the second paper.

We are currently extending the present HTSE calculation to compute the critical temperature of ferromagnets of $J = 2$ and $\frac{5}{2}$ in a cubic crystal field of arbitrary strength. To generalize the present formulation for the antiferromagnetic systems is also of immediate interest.

ACKNOWLEDGMENTS

This work is supported by NSF Grant No. DMR 77-21539. We are also grateful to the Florida State University Computing Center for making available to us the needed computer time.

[1]For a review see B. R. Cooper, in *Magnetic Properties of Rare Earth Metals,* edited by R. J. Elliott (Plenum, New York, 1972). Also P. Fulde and I. Peschel, Adv. Phys. 21, 1 (1972).
[2]Y. L. Wang, Solid State Commun. 10, 533 (1972).
[3]W. Wuchner, and J. Langsch, Int. J. Magn. 5, 181 (1973).
[4]R. Elliott, R. T. Harley, W. Hayes, and S. R. P. Smith, Proc. R. Soc. London A 328, 217 (1972).
[5]Y. L. Wang, and B. R. Cooper, Phys. Rev. 172, 539 (1968); 185, 696 (1969).
[6]D. A. Pink, J. Phys. C 1, 1246 (1968).
[7]R. J. Elliott and C. Wood, J. Phys. C 4, 2359 (1971). J. Oitmaa and M. Plischke, J. Phys. C 9, 2093 (1976).
[8]B. D. Rainford and J. G. Houmann, Phys. Rev. Lett. 26, 1254 (1971).
[9]E. Bucher, C. W. Chu, J. P. Maita, K. Andres, A. S. Cooper, E. Buehler, and K. Nassau, Phys. Rev. Lett. 22, 1260 (1969).
[10]R. J. Birgeneau, J. Als-Nielsen, and E. Bucher, Phys. Rev. Lett. 27, 1530 (1971); Phys. Rev. B 6, 2724 (1972).
[11]K. Andres, E. Bucher, S. Darack, and J. P. Maita, Phys. Rev. B 6, 2716 (1972); E. Bucher, J. P. Maita, and A. S. Cooper, Phys. Rev. B 6, 2709 (1972).
[12]T. M. Holden, E. C. Svenssen, and W. J. L. Buyers, Phys. Rev. B 10, 3864 (1974).
[13]Y. Y. Hsieh and M. Blume, Phys. Rev. B 6, 2684 (1972).
[14]Y. L. Wang and F. Lee, Phys. Rev. Lett. 38, 912 (1977).
[15]R. P. Guertin, J. E. Crow, F. P. Missell, and S. Foner, Phys. Rev. B 17, 2183 (1978).
[16]K. R. Lea, M. J. M. Leask, and W. P. Wolf, J. Phys. Chem. Solids, 23, 1381 (1962).
[17]A. L. Fetter and J. D. Walecka, *Quantum Theory of Many-Particle Systems* (McGraw-Hill, New York 1971).
[18]V. G. Vaks, A. I. Larkin, and S. A. Pikin, Ah. Eksp. Teor. Fiz. 53, 281 (1967) [Sov. Phys. JETP 26, 188 (1968)].
[19]D. H. Yang and Y. L. Wang, Phys. Rev. B 10, 4714 (1974).
[20]S. B. Haley and P. Erdos, Phys. Rev. B 5, 1106 (1972).
[21]For results of anisotropic exchange interactions see K. Rauchwarger, Dissertation 1978 (unpublished).
[22]B. R. Cooper, Phys. Rev. B 6, 2730 (1972).